

## Feasibility study on Hartman–Schijve data analysis for mode II fatigue fracture of adhesively bonded wood joints

Clerc, Gaspard; Brunner, Andreas J.; Niemz, Peter; Van de Kuilen, Jan Willem G.

**DOI**

[10.1007/s10704-019-00414-5](https://doi.org/10.1007/s10704-019-00414-5)

**Publication date**

2019

**Document Version**

Final published version

**Published in**

International Journal of Fracture

**Citation (APA)**

Clerc, G., Brunner, A. J., Niemz, P., & Van de Kuilen, J. W. G. (2019). Feasibility study on Hartman–Schijve data analysis for mode II fatigue fracture of adhesively bonded wood joints. *International Journal of Fracture*, 221 (2020)(2), 123–140. <https://doi.org/10.1007/s10704-019-00414-5>

**Important note**

To cite this publication, please use the final published version (if applicable). Please check the document version above.

**Copyright**

Other than for strictly personal use, it is not permitted to download, forward or distribute the text or part of it, without the consent of the author(s) and/or copyright holder(s), unless the work is under an open content license such as Creative Commons.

**Takedown policy**

Please contact us and provide details if you believe this document breaches copyrights. We will remove access to the work immediately and investigate your claim.

## Feasibility study on Hartman–Schijve data analysis for mode II fatigue fracture of adhesively bonded wood joints

Clerc, Gaspard; Brunner, Andreas J.; Niemz, Peter; Van de Kuilen, Jan Willem G.

**DOI**

[10.1007/s10704-019-00414-5](https://doi.org/10.1007/s10704-019-00414-5)

**Publication date**

2019

**Document Version**

Final published version

**Published in**

International Journal of Fracture

**Citation (APA)**

Clerc, G., Brunner, A. J., Niemz, P., & Van de Kuilen, J. W. G. (2019). Feasibility study on Hartman–Schijve data analysis for mode II fatigue fracture of adhesively bonded wood joints. *International Journal of Fracture*, 221 (2020)(2), 123–140. <https://doi.org/10.1007/s10704-019-00414-5>

**Important note**

To cite this publication, please use the final published version (if applicable). Please check the document version above.

**Copyright**

Other than for strictly personal use, it is not permitted to download, forward or distribute the text or part of it, without the consent of the author(s) and/or copyright holder(s), unless the work is under an open content license such as Creative Commons.

**Takedown policy**

Please contact us and provide details if you believe this document breaches copyrights. We will remove access to the work immediately and investigate your claim.



# Feasibility study on Hartman–Schijve data analysis for mode II fatigue fracture of adhesively bonded wood joints

Gaspard Clerc · Andreas J. Brunner · Peter Niemz · Jan Willem G. Van de Kuilen

Received: 18 August 2019 / Accepted: 10 December 2019 / Published online: 19 December 2019  
© Springer Nature B.V. 2019

**Abstract** The feasibility of using the modified Hartman–Schijve (HS) equation to analyze the fatigue fracture performance of adhesively bonded wood specimens under cyclic mode II loading was investigated in comparison with the Paris crack growth equation. Wood joints prepared with three different adhesives have been subject to cyclic Mode II testing at room-temperature (23 °C and 50% relative humidity) in a four-point End-Notched-Flexure configuration, determining the crack length from specimen compliance. It was shown, that the HS-equation can be successfully applied to adhesively bonded wood and that it successfully estimates threshold and maximum energy release rate (ERR) values for three different adhesive systems. Since a limited number of tests were performed for investigating the feasibility, scatter sources and pos-

sible scatter reduction methods are analyzed and discussed in detail. Also, a new, automated data reduction method was developed for estimating the maximum and the threshold ERR ( $G_{thr}$ ) values. The main advantage of the HS-equation appears to be the application in design standards. However, before the maximum ERR and  $G_{thr}$  values derived here can be used in design applications or for drafting a design guideline, additional testing is required for understanding how the number of cycles, the related measurement resolution; the corresponding ERR value influence the threshold value  $G_{thr}$  and how and to what extent its scatter can be reduced; and to further explore the link between cyclic ERR and the critical ERR value measured during quasi-static fracture tests.

G. Clerc (✉) · P. Niemz  
Bern University of Applied Sciences, Architecture, Wood and Civil Engineering, Solothurnstrasse 102, 2500 Biel, Switzerland  
e-mail: gaspard.clerc@bfh.ch

A. J. Brunner  
Empa, Swiss Federal Laboratories for Materials Science and Technology, Mechanical Systems Engineering, Überlandstrasse 129, 8600 Dübendorf, Switzerland

G. Clerc · J. W. G. Van de Kuilen  
Technical University of Munich, Wood Research Munich (HFM), Winzererstrasse 45, 80797 Munich, Germany

J. W. G. Van de Kuilen  
Delft University of Technology, Faculty of Civil Engineering and Geosciences, Biobased Structures & Materials, 2628 CN Delft, The Netherlands

**Keywords** Wood adhesive · Fatigue fracture · 4-ENF · Paris-plot · Hartman–Schijve equation

## 1 Introduction

Timber as a renewable carbon-neutral material is gaining interest in the field of construction trying to reduce its ecological impact. To assure the future of timber as construction material, a good understanding of its mechanical behavior is required to obtain design rules that are not too conservative. In this matter, the design rules considering the fatigue behavior of timber generally are based on an extremely conservative design (Lewis 1960). Furthermore, the influence of adhesive

on the fatigue life generally is not considered due to the lack of research in this domain (Kyanka 1980). Also, most of the research considering the fatigue life of wood (Aicher 2015; Smith et al. 2003), or bonded wood (Bachtiar et al. 2017) is based on stress-cycle (S–N) tests, the aspect of crack propagation under fatigue loading of wood or bonded wood has received scant attention at best. Recently, Clerc et al. (2019a, b) showed that the fatigue crack-growth of adhesively bonded wood joints is successfully described by the Paris equation (Paris and Erdogan 1963) in the linear part of a fatigue test. Further, the type of adhesive has an influence on the crack growth rate, with ductile adhesives showing typically a faster delamination propagation compared to brittle adhesive systems. Since the Paris equation was originally developed to describe fatigue phenomena in metallic material, the stress intensity factor  $K$  was used. For composite materials, the use of the energy release rate (ERR), i.e., the  $G$ -value, is preferred over the stress intensity factor due to the material anisotropy. There is, however, still no consensus on whether it is more appropriate to use  $G_{\max}$ ,  $\Delta G$  or  $\Delta\sqrt{G}$  or a combination thereof (Alderliesten et al. 2018). However, as the Paris-equation (in a double-logarithmic presentation) can only be used to describe the linear range of crack growth during a fatigue test, it does not provide direct information for estimating a threshold energy release rate ( $G_{\text{thr}}$ ) or the maximum energy release rate. These values, however, constitute essential information for the future development of a design standard considering the behavior of adhesively bonded wood over the complete fatigue crack propagation range. To extend the Paris-equation beyond the linear fatigue crack growth range, Hartman and Schijve (1970) proposed a new equation for the study of aluminum alloys which was adapted by Jones et al. (2012) as modified Hartman–Schijve (HS) equation to represent Mode I, Mode II, and later Mode I/II delamination growth in composites, as shown in Eq. (1).

$$\frac{da}{dN} = D \left( \frac{\sqrt{G_{\max}} - \sqrt{G_{\text{thr}}}}{\sqrt{1 - \sqrt{G_{\max}/A}}} \right)^{\beta} \quad (1)$$

where  $a$  is the crack length,  $N$  the number of cycles,  $G_{\max}$  the maximum ERR measured during one cycle,  $G_{\text{thr}}$  the threshold ERR value,  $A$  the maximum ERR value and  $D$ ,  $\beta$  being fit parameters.

The advantage of the HS-equation is that it describes the full fatigue life of the specimen in a single, roughly linear equation whereas the Paris-equation describes only a limited part of crack growth (Jones et al. 2012). Furthermore, the HS-equation is capable of accounting for R-ratio effects. The HS-analysis uses a transformation of the x-axis where two additional parameters are introduced,  $G_{\text{II,thr}}$  a threshold ERR value and  $A$  the maximum ERR value for Mode II, the latter roughly corresponding to the critical ERR obtained during quasi-static tests. One further advantage of using the HS-equation is that the complete data set can be directly used for analysis. In comparison, data analyzed with the Paris equation should be carefully chosen so that only the linear part of crack growth is analyzed. Despite these advantages, a more refined data reduction method is needed to be able to estimate the four parameters needed for the HS-equation with sufficient accuracy (instead of two for the Paris equation).

Of the four parameters in the HS-equation, two are fitting constants, i.e.,  $D$  and  $\beta$  that are analogous to the  $C$  and  $m$  coefficients of the Paris-equation as described by Clerc et al. (2019a, b) and two are constants that each can be associated with a physical phenomenon. As explained previously the  $A$  value can be associated with the onset of crack growth corresponding approximately to the critical ERR obtained during quasi-static test ( $G_{5\%}$ ). The  $G_{\text{II,thr}}$  value, in principle, corresponds to the minimum ERR below which no crack growth should happen. It, together with the associated scatter, represents therefore a very important quantity for design purpose (Jones et al. 2017). Several different methods exist to determine these values (Yao et al. 2018), which are generally based on the same idea, i.e., obtaining a linear ‘master’ relationship between the ERR and  $da/dN$  values by adjusting the  $A$  and  $G_{\text{II,thr}}$  values. This can be easily accomplished for data with comparatively low scatter as it is generally the case in polymer composites. But for adhesively bonded wood specimens, due to higher scatter of the data, a new automated method was developed in this paper.

Beside the limited number of specimens tested in the feasibility study, the underlying reasons for the relatively high scatter observed in the results are not yet completely understood. Likely, these are due to a number of factors. Alderliesten et al. (2018) classify these into intrinsic and extrinsic factors (cite): ‘‘Examples of the latter are test set-up (e.g., compliance or play in the load-introduction, or load cell range with insuf-

cient measurement resolution), operator experience (e.g., learning curve for proper test set-up as well as visual observation during testing), but also machining variation in specimen width and cutting quality, or variation in laminate plate thickness (e.g., near the edges) affecting the individual specimens' compliance which should be limited or excluded by proper test specification. The intrinsic scatter, i.e. due to processing variability and inhomogeneous material morphology, should be considered relevant for design purposes and shall not be excluded nor underestimated." In addition to the extrinsic scatter observed during fatigue fracture testing, wood itself is known to have a higher variability in morphology and hence yields higher intrinsic scatter in properties and fracture behavior than polymer composite materials.

During a real fatigue test, the crack growth does not always follow a continuously increasing path. During short time intervals, the crack can quickly grow and then stabilize before following the same tendency again. During these sporadic events, the crack growth rate and the energy level will change abruptly. If plotted chronologically in a double logarithmic plot, the obtained energy level and crack growth rate during these sporadic events strongly deviate from the average as their values are much higher and lower, respectively. This problem is generally best solved by fitting the crack length and the ERR data using an equation such as a second order power model (Stelzer et al. 2014). This, however, has the effect where all the sporadic events are smoothed to some extent by the fitting procedure, allowing, on the other hand, the scatter to be drastically reduced. It is, however, questionable to eliminate a source of scatter without determining its origin. Indeed, if the irregular crack growth events are due to material heterogeneity or non-uniform adhesive distribution, these shall be considered as intrinsic scatter and not be eliminated. Furthermore, as shown by Clerc et al. (2019a, b), the fit quality of a second order power model at the beginning and at the end of the test is generally low. This may not be an issue if the data are represented using the Paris-equation, where the main interest lies in the linear part of the test and the fit of the power model is generally good. However, if the data are plotted using the HS-equation, the test behavior should be accurately described, also for low and high ERR in order to be able to reliably determine the values of  $A$  and  $G_{\text{thr}}$ .

Clerc et al. (2019a, b) present a simple method based on a moving average (on a logarithmic scale) of the

crack growth rate and maximum ERR per cycles to estimate the Paris coefficient. This method is developed further in this paper to allow for an automatic estimation of the HS-parameters. A specific focus was given to the estimation of the ERR threshold and maximum value ( $A$  and  $G_{\text{II,thr}}$ ), as they correspond to physical quantities which can be used for development of a future design standard.

The goal of this article is to examine if the HS-equation can be successfully applied to adhesively bonded wood and to compare the analysis of mode II fatigue crack growth data using the Paris-equation and the HS-equation in order to establish the strengths and weaknesses of both approaches as well as to validate approaches for reducing extrinsic scatter in the data.

In Sect. 2, the preparation of the samples and the testing method will briefly be summarized. Then the data reduction method and the method used to determine the  $A$  and  $G_{\text{thr}}$  value are presented in detail. These methods then are applied in Sect. 3 to adhesively bonded wood glued with three different adhesive systems and tested with the four point End-Notched Flexure (4-ENF) specimen in constant amplitude cyclic fatigue. In Sect. 4, the sources of scatter will be discussed, and a different method will be presented with the potential of reducing the scatter of the data. Finally, in the conclusion, the main findings in this article will be summarized and a brief outlook will be given on how to improve the results presented here and how they can possibly be used in a design guideline.

## 2 Material and methods

### 2.1 Preparation of the samples

A detailed description of the samples' preparation and the testing method can be found in Clerc et al. (2019a, b). Only the main steps will be described here. Beech wood (*Fagus sylvatica* L.) with a mean density of  $714 \text{ kg/m}^3$  at a wood moisture content of 12% was used for the tests. The wood had no defects such as knots and grain deviation, the boards were planed prior to bonding to avoid the migration of wood extractives on the surface and to guarantee their planeness. Before the adhesive bonding, a  $15 \text{ }\mu\text{m}$  thick fluoropolymer (ETFE230N) foil was applied between the lamel-

lae on the first 120 mm to simulate a starter crack. Three adhesives are compared in the tests, one relatively brittle phenol resorcinol formaldehyde (PRF, trade name «Aerodux 185») with a Young's modulus of approx. 2750 MPa and two ductile one component polyurethane (1C-PUR) adhesives with a low Young's modulus (approx. 1000 MPa for the VN3158 and 500 MPa for the HB 110). These two 1C-PUR adhesives are based on the same polymer, with the difference that additional small polyamide fibers were introduced in the adhesive matrix of the LOCTITE HB 110 PUR-BOND and not in the LOCTITE VN 3158. The adhesives were pressed during 10 hours at a pressure of 1 MPa and at a temperature of approx. 20 °C. Once cured, the front-position of the foil was referenced as position of the crack tip and the crack length was set to 110 mm. The samples were then cut to a width of 20 mm and a length of 317 mm. The adhesively bonded wood joints were stored for several days in the test climate of 23 °C and 50% relative humidity before testing.

## 2.2 Testing method

The setup used for this experiment is schematically shown in Fig. 1.

In Fig. 1,  $P$  is the load,  $P_L$  and  $P_R$  the relative loads under both loading points.  $V_L$  and  $V_R$  are the displacements under both loading points. Due to the pinned configuration, the force  $P_L$  is equal to  $P_R$ . The compliance at the loading point is then defined as the ratio of displacement to the applied force, which corresponds to Eq. (2). Only the main equations are summarized here, a detailed derivation can be found in Clerc et al. (2019a, b).

$$C_c = \frac{\delta_c}{P} = \frac{49L^2(L + 54a)}{10368EI} \quad (2)$$

The energy release rate  $G_{II}$  is calculated according to Eq. (3):

$$G_{II} = \frac{P^2}{2b} \frac{dC}{da} = \frac{49}{384} \frac{P^2 L^2}{BEI} \quad (3)$$

The crack length is calculated from the compliance Eq. (4)

$$a = \frac{C_c \cdot 10368 \cdot EI - 49L^3}{2646L^2} \quad (4)$$

The MOE was calculated according to Eq. (5) at a load of  $P = 200$  N (higher than the initial deformation of

the setup and lower than the crack start, and hence in the elastic range).

$$E = \frac{49L^3 + 2646L^2 a_0}{10368C_0 I} \quad (5)$$

## 2.3 Evaluation of the quasi-static samples

The ERR was computed at two different load points. The first point ( $P_{NL}$ ) corresponds to the point of initiation of the crack propagation, it is defined as the limit of the elastic range. With this point, the slope of the elastic part is calculated. The crossing point between a 5% more compliant slope and the load-deformation curve is then obtained as a second point ( $P_{5\%}$ ).

## 2.4 Evaluation of the cyclic fatigue loaded samples

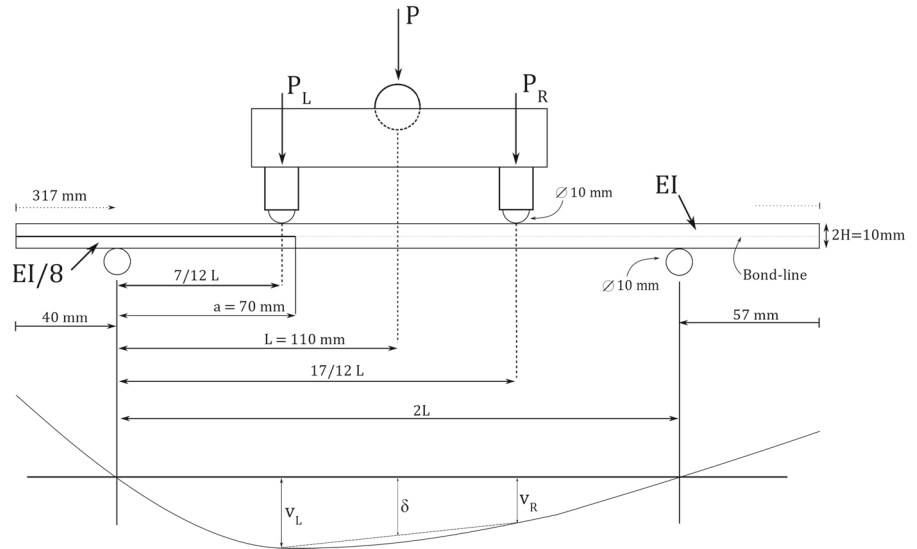
A similar evaluation method was used as for the quasi-static tested samples. As suggested by Simon et al. (2017) the compliance of the samples is calculated with:

$$C = \frac{\delta_{max} - \delta_{min}}{P_{max} - P_{min}} \quad (6)$$

where  $\delta_{max}$  and  $\delta_{min}$  correspond to the maximum and minimum displacement, and  $P_{max}$  and  $P_{min}$  to the maximum and minimum force value per cycle, respectively.

The main difficulty regarding the analysis of the samples consists of the smoothing of the data affected by experimental scatter. During the test, maximum and minimum force and displacement values were recorded. The data were then smoothed using the "logarithmic fitting" algorithm described by Clerc et al. (2019a, b). For example, data-points are averaged every 200 cycles until 1000 cycles then every 500 cycles until 10,000 then every 1000 cycles until the end of the test. These "cycle range" parameters were adjusted according to the different samples to obtain regularly spaced points over the test and a comparable number of data-points between the different samples. The compliance-data calculated according to Eq. (6) were log-fitted before calculating the crack length and its corresponding derivative. The ERR data, calculated according to Eq. (3) was also log-fitted with the same parameters as the compliance data.

**Fig. 1** Schematic representation of the test setup drawn to scale with theoretical deformation line, the total crack length is 110 mm measured from the left side of the specimen—an hinge was used to distribute the force equally between  $P_L$  and  $P_R$ —testing setup according to Clerc et al. (2019a, b)



## 2.5 Testing procedure

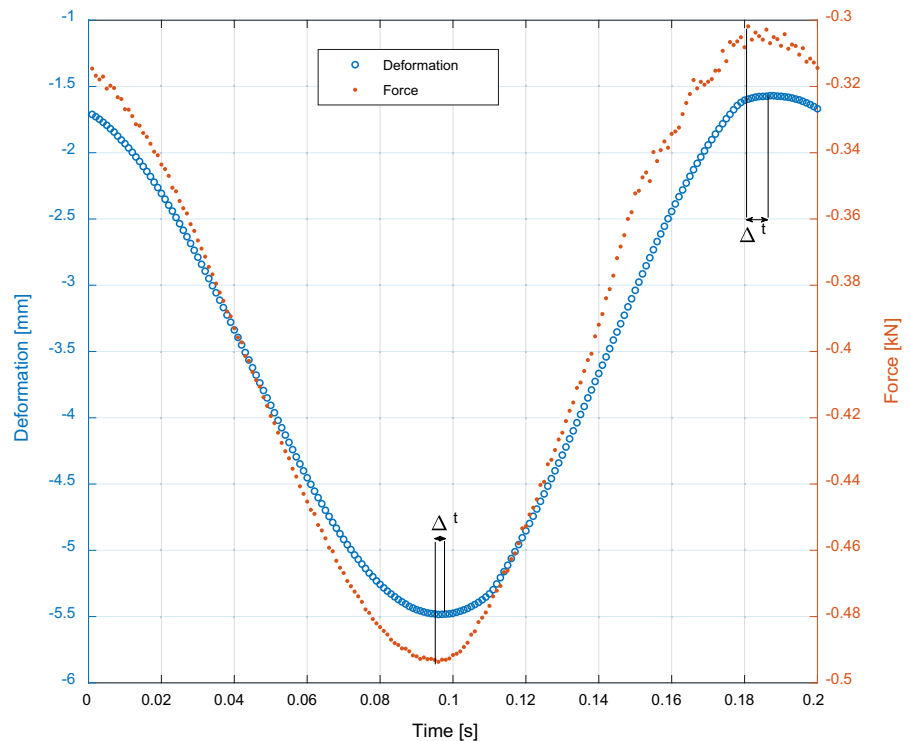
The machine used for the test was a servo-hydraulic test machine (type 1237 Instron) equipped with a 1 kN load cell. The head of the support was fully articulated to prevent any bending moment in the fixture apparatus. The quasi-static tests were performed under displacement control at 1 mm/min. For the cyclic loaded samples, three samples for each adhesive were tested at a frequency of 5 Hz under displacement-control until reaching 40,000 cycles or until a very slow crack growth was reached. The average machine displacement value was fixed to 13.36 mm corresponding approximately to the average force observed at the  $P_{NL}$ -point. The displacement amplitude was set to  $\pm 2.1$  mm corresponding approximately to a force of  $\pm 200$  N. A few extra supports were placed to prevent the sample from sliding during the test and Teflon was sprayed on the sample for assuring a low friction between the sample and the machine support.

## 2.6 Sources of extrinsic scatter

The load and displacement were measured with an accuracy of 1% of the measured value, meaning that the force was measured with an accuracy of at least 5 N and the displacement with an accuracy of 0.1 mm. The compliance of the setup was corrected using a stiff steel bar for calibration (Clerc et al. 2019a, b). The non-linear initial play in the setup was corrected by extending

the linear elastic part of the load–displacement curve to the crossing point with the deformation axis. During the test, only the maximum and minimum displacement and load values per cycle were recorded to limit the data file size. In order to check the accuracy of the maximum and minimum values preliminary tests were recorded during a few cycles with a 1 kHz sampling rate, meaning that on average 200 data points were recorded per cycle. An average step of 4 N (and 0.042 mm) between two successive data points was observed over the complete cycle, but well below that near the maximum and minimum value (Fig. 2). This inaccuracy was estimated to be below 0.1 N and 0.01 mm. A potential source of systematic error could be the fact that the maximum and minimum force and displacement values per cycle were not necessarily recorded at the same time. As shown in Fig. 2, there is a phase difference between the force and deformation data. Where the maximum deformation appears before the maximum force, the difference is less for the minimum value per cycle. By averaging the behavior of the specimen over one cycle and using only the maximum and minimum value, a time difference of approximately 0.004 s could be observed between the maximum values of the displacement and force data. This means, that the compliance is not necessarily estimated at the exact same time, the influence of this systematic error on the result is however difficult to estimate. Using these rough estimates, the accuracy of the compliance is estimated to be 2.3% if the compliance is calculated as  $C = \delta_{max}/P_{max}$  and 4.3 % if

**Fig. 2** Phase difference between the force and deformation measurement during one cycle illustrating that there is a time delay between the maximum and minimum force and deformation values, meaning that they are not necessarily measured at the exact same time



the compliance is calculated using Eq. 6. In both cases, the accuracy of the load cell is dominant accounting for 80% of the inaccuracy.

## 2.7 Fitting process for samples tested under cyclic fatigue loading

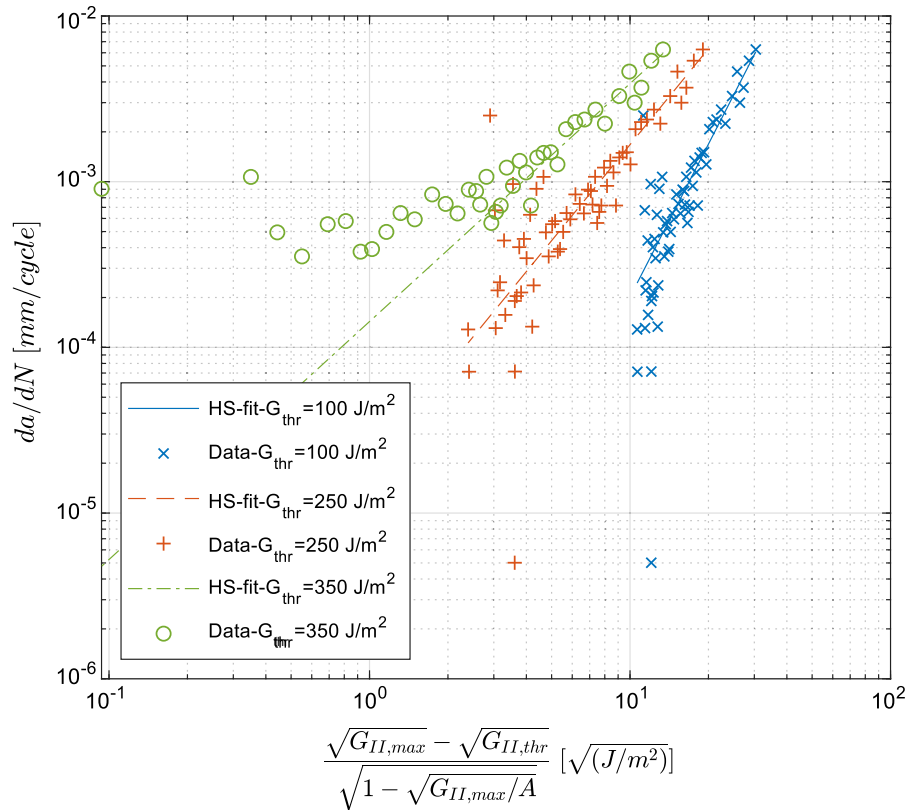
### 2.7.1 General procedure

The fitting procedure consisted of two steps, a first fit was done to calculate the value of  $A$  and  $G_{II,thr}$ , without considering the influence of  $D$  and  $\beta$ . Then, using the values of  $A$  and  $G_{II,thr}$ , a second fit was done to obtain the value for  $D$  and  $\beta$ . One can see in Eq. 1 that for  $G_{II}$  term near  $G_{II,thr}$ , the  $x$ -axis will tend to zero crack growth rate. Additionally,  $G_{II,max}$  values smaller than  $G_{II,thr}$  are resulting in a negative crack growth rate. A  $G_{II,max}$  value near the  $A$  value will tend to infinity, meaning a virtually infinite crack growth rate. Therefore, as first estimation the  $G_{II,thr}$  value should be lower than the maximum ERR value obtained for each cycle ( $G_{II,max}$ ) and the  $A$  value should be higher than the  $G_{II,max}$  values. Furthermore, as the HS-equation (1) is covering the entire fatigue-life of the sample, all the

data points shall be displayed on a straight line. This can be achieved, as suggested by Jones et al. (2014), by plotting the  $da/dN$  values and the term  $\left(\frac{\sqrt{G_{max}} - \sqrt{G_{thr}}}{\sqrt{1 - \sqrt{G_{max}/A}}}\right)$  on a double logarithmic scale as shown in Fig. 3 and by adjusting the  $A$  and  $G_{II,thr}$  coefficients. By choosing the appropriate value of  $G_{II,thr}$ , the non-linearity of the data in the threshold domain can be reduced. For example, in Fig. 3, a  $G_{II,thr}$  value of  $100 \text{ J/m}^2$  is too low as the data-points are shifted on the right-side of the line. The contrary is observed for a  $G_{II,thr}$  value of  $350 \text{ J/m}^2$  as this time the data are shifted to the left-side of the line. A  $G_{II,thr}$  value of approximately  $250 \text{ J/m}^2$  seems here a reasonable estimate as the data are following a fairly linear trend.

The starting value of  $A$  is based on the ERR measured at  $P_{5\%}$  under quasi-static loading. The upper bound for estimating the  $A$  value was fixed at two standard deviations from the average  $G_{II,5\%}$  value, the lower bound was fixed to be the maximal ERR release rate measured during the fatigue cyclic tests (as theoretically the  $A$  value cannot be smaller than the maximum ERR measured during the test). The lower bound for estimating the  $G_{thr}$  value was set to zero and the upper

**Fig. 3** Influence of the variation  $G_{II,thr}$  value for one sample glued with the adhesive HB 110 using the HS-analysis—a  $G_{II,thr}$  value of  $100 \text{ J/m}^2$  is too low as the data-points are shifted on the right-side of the line. The contrary is observed for a  $G_{II,thr}$  value of  $350 \text{ J/m}^2$  as this time the data are shifted to the left-side of the line. The most representative  $G_{II,thr}$  value should result in the data point being plotted along a straight line as shown with  $G_{II,thr} = 250 \text{ J/m}^2$



bound to the minimum ERR value measured during the test.

2.7.2 Automatic method for estimating the  $A$  and  $G_{thr}$  value

Using the above-mentioned procedure to estimate “manually” the value of  $A$  and  $G_{thr}$  is a rather cumbersome and subjective process as due to the scatter of the data it is difficult to judge if the data are forming a straight line. For this reason, a simple procedure was proposed to automatically estimate the value of  $A$  and  $G_{thr}$ . Using the above-mentioned assumption, it is possible to design an algorithm generating random values (from a uniform distribution) of  $A$  and  $G_{thr}$  which control if the data are forming a straight line. For each random pair of  $A$  and  $G_{II,thr}$  the term  $\left(\frac{\sqrt{G_{max}} - \sqrt{G_{thr}}}{\sqrt{1 - \sqrt{G_{max}}/A}}\right)$  is computed and fitted using the HS-equation (3). As evaluation criteria, the coefficient of determination (CoD) is calculated for each pair. Then the highest CoD values, and the corresponding  $A$  and  $G_{thr}$  values are selected as they should represent the best fit. An example of the

$A$  and  $G_{thr}$  value obtained with this method is shown in Fig. 4. In this contour plot, the coefficients are shown in a color scale on the right of the picture (the scale is truncated to show only high CoD values). Even though the differences in the CoD are relatively small, a clear tendency can be seen leading to a best fit in this example of  $706.2 \text{ J/m}^2$  for  $A$  and  $261.2 \text{ J/m}^2$  for  $G_{thr}$  with a CoD of 0.8209. Due to the random nature of the estimation, the best fit is not always located exactly at the same place. To estimate the variability of the best fit, ten different random initializations (with 2500  $A$  and  $G_{thr}$  pairs each) are done and the average and standard deviation of the best fitting  $A$  and  $G_{thr}$  values are calculated. Using this method for each tested sample, 25,000 pairs of  $A$  and  $G_{thr}$  are randomly generated giving a coefficient of variation of approximately 5% for the  $A$  and  $G$  values. The average coefficient of variation for the CoD value was below 0.1%.

The contour plot shown in Fig. 4, can also be used as sensibility analysis tool for estimating the influence of a relative change in the  $A$  and  $G_{thr}$  values. In Table 1, the influence of a 5% and 10% higher or lower  $A$  or  $G_{thr}$  value (keeping respectively the  $G_{thr}$  or  $A$  value

**Fig. 4** Contour plot of the coefficient of determination corresponding to different A and  $G_{thr}$  values. For this sample glued with the adhesive HB 110, the best CoD (0.8209) is obtained with a value of 706.2  $J/m^2$  for A and 261.2  $J/m^2$  for  $G_{II,thr}$ . The color-scale is truncated to show only the high CoD values

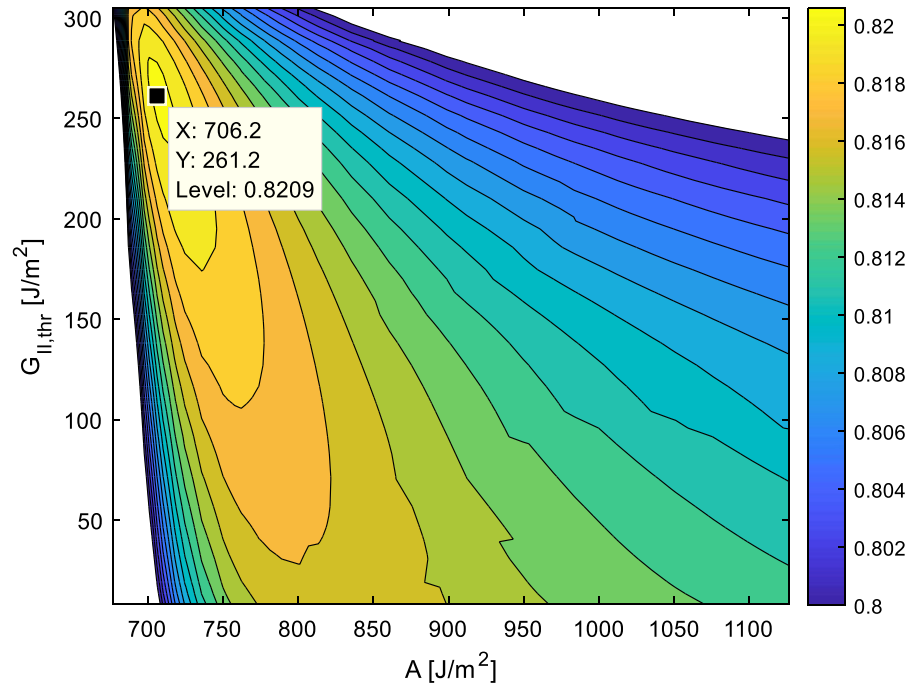


**Table 1** Influence of a variation of  $\pm 5\%$  and  $\pm 10\%$  on the value of  $G_{thr}$  and A on the CoD—data set obtained from one sample glued with the adhesive HB 110—\*A-10% would be lower than the maximum ERR measured during the test hence resulting in a negative value and was therefore not calculated

	A ( $J/m^2$ )	$G_{thr}$ ( $J/m^2$ )	CoD
Ref.	723	246	0.8205
A + 5%	760	246	0.8166
A - 5%	687	246	0.8109
$G_{thr} + 5\%$	723	258	0.8200
$G_{thr} - 5\%$	723	234	0.8204
A + 10%	795	246	0.8141
$G_{thr} + 10\%$	723	271	0.8193
$G_{thr} - 10\%$	723	221	0.8204

constant) can be seen. It appears that a relative change of the A value has more influence than of the  $G_{thr}$  value. This can also be observed in Fig. 4, where all the range of the tested  $G_{thr}$  value can give a CoD higher than 0.81 (if the appropriate A value is chosen). Whereas, a small decrease of the A value promptly results in a low CoD.

### 2.7.3 Influence of the data-reduction method on the A and $G_{thr}$ value

To evaluate the influence of the number of data points on the estimation of the A and  $G_{thr}$  values, two different data reduction methods were compared. The first data set (labeled “LogFit1”) is obtained by averaging the data every 100 cycles until 1000, every 200 cycles until 10,000 and every 400 cycles until the end of the test, giving a total data set of 161 data points. Clerc et al. (2019a, b) provide a more detailed description of the data reduction method. The second data set (labeled “LogFit 2”) is obtained by averaging the data every 100 cycles until 1000 cycles, every 300 cycles until 10,000 and every 600 cycles until the end of the test giving a total data set of 110 data points. For the data set LogFit 1 and LogFit 2 the above described procedure (Sect. 2.7.2) was used to estimate the value of A and  $G_{thr}$ . The numerical values obtained with a 95% confidence interval are shown in Table 2.

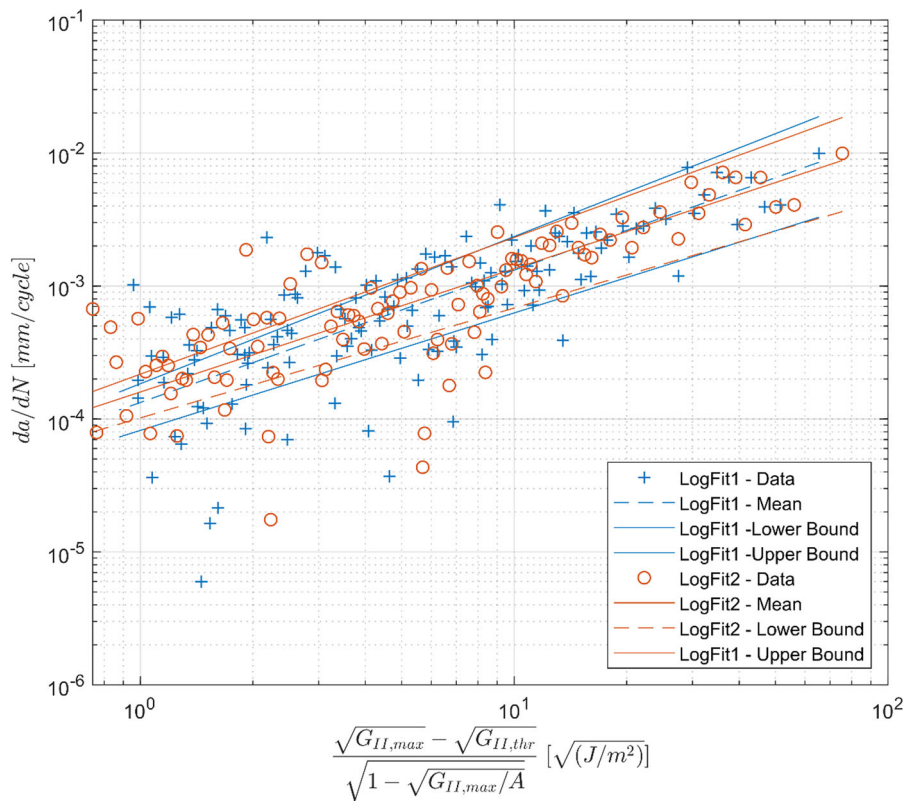
The difference between both A and  $G_{thr}$  values estimated from different LogFit data set, are in the 95% confidence interval (see Fig. 5). However, the A value is slightly higher in the LogFit1 data-set whereas the  $G_{thr}$  value from Logfit1 is slightly lower. This is probably explained by the non-equivalent weighting of the

**Table 2** Numerical values of A, G<sub>thr</sub>, D and β values for two different LogFit data sets obtained from one sample glued with the adhesive HB 110

		Mean	Lower bound (95% confidence interval)	Upper bound (95% confidence interval)
Data Set “LogFit1”	A (J/m <sup>2</sup> )	894	876	912
	G <sub>thr</sub> (J/m <sup>2</sup> )	307	297	317
	D (mm/cycle)	1.331E−3	8.207E−05	1.842E−04
	β[−]	0.995	0.8833	1.107
Data Set “LogFit2”	A [J/m <sup>2</sup> ]	879	865	894
	G <sub>thr</sub> (J/m <sup>2</sup> )	313	301	325
	D (mm/cycle)	1.596E−3	1.019E−04	2.174E−04
	β[−]	0.9271	0.8264	1.028

Range is given with a 95% confidence interval

**Fig. 5** Comparison of the same sample with two different LogFit parameters (see text) to illustrate the influence of the number and repartition of data points on the determination of the A and G<sub>thr</sub> values—the upper and lower bound for each LogFit are given with a 95% confidence interval



different parts of the test. For both data sets the moving average parameters were equivalent until 1000 cycles, only after that were the number of data points reduced in the LogFit2 data set. This implies, that the data set LogFit1 has proportionally more data in the upper part of the test than the logFit2 data set. This probably explains why, having relatively more data in the upper range of

the test, the A value is higher (and the G<sub>thr</sub> value lower) in the LogFit1 Data Set.

Despite these small differences, the fits are considered similar between both data sets with a CoD of 0.7022 for the Data set “LogFit1” and 0.8039 for the data set “LogFit2”. The parameters corresponding to this data set were chosen for further analysis due to the higher CoD.

### 3 Results

#### 3.1 Quasi-static loading

The ERR measured at the  $P_{5\%}$  points under quasi-static loading was  $896 \pm 120 \text{ J/m}^2$  for the samples glued with the HB 110 adhesive,  $1004 \pm 77 \text{ J/m}^2$  for the PRF adhesive and  $1023 \pm 131 \text{ J/m}^2$  for the VN 3158 adhesive (from Clerc et al. (2019a, b)).

#### 3.2 Cycle-fatigue loading

The above-mentioned method will be tested on adhesively bonded specimen bonded with different types of adhesive. In Fig. 6, the fatigue test results of all samples glued with the adhesive HB 110 are presented. The fit parameters obtained for each sample are shown in Table 3.

The general slope is very similar between the three samples but still, significant scatter can be noted for the sample HB3. The cause for this scatter will be further discussed. The obtained HS parameters are relatively similar, with an average  $A$  value of  $785 \text{ J/m}^2$  and an average  $G_{\text{thr}}$  value of  $285 \text{ J/m}^2$ .

For the VN adhesive, the samples VN2 and VN3 show a very similar behavior (see Fig. 7). However the sample VN-1 presents a different slope and a comparatively higher  $G$  value as the other samples glued with the VN adhesive. The same tendency could be observed for this sample in Clerc et al. (2019a, b). For all samples glued with the VN, an important scatter is also observed. It shall also be noted that the average slope for the VN samples is similar to the HB 110 samples. However, the average value of  $A$  ( $1228 \text{ J/m}^2$ ) is significantly higher for the VN adhesive than for the HB 110 adhesive. The same tendency was observed during the quasi-static test where a higher maximum ERR value was measured for the VN samples. In comparison, the average threshold ERR value ( $192 \text{ J/m}^2$ ) is clearly lower than for the HB 110 samples.

Only two samples glued with the adhesive PRF could be successfully analyzed with the above-mentioned method. For the sample PRF1, no satisfying results could be obtained using the random estimation of the  $A$  and  $G$  value. This is probably due to the short delamination (only 16,000 cycles compared to the 40,000 cycles for the other samples). Indeed, if too few points are available for the fitting algorithm, no CoD can suc-

cessfully be calculated resulting in a failed estimation. Increasing the moving average filter parameters to obtain more data points, was in this case not successful as this tended to increase the scatter even more. It can, however, be seen in Fig. 8 that the data points are matching relatively well the other tested PRF samples. The average  $A$  ( $880 \text{ J/m}^2$ ) and  $G_{\text{thr}}$  ( $552 \text{ J/m}^2$ ) values obtained for the PRF2 and PRF3 samples were used to plot the data of the sample PRF1.

For the PRF samples, the average  $A$  value is similar to the one obtained for the HB 110 samples but clearly lower than for VN samples. The PRF samples are showing the highest  $G_{\text{thr}}$  and  $A$  values in comparison with both 1C-PUR adhesives. Meaning that in average, a slower crack growth will be observed for specimen glued with this adhesive, and that the crack growth will become infinitely small at a higher energy than for the other adhesives tested in this study.

In order to allow for a better comparison between the adhesive performances, all the data samples are plotted together in Fig. 9. Each sample was plotted using the value of  $A$  and  $G_{\text{thr}}$  determined in Table 3. Then, all the data for one adhesive system are combined in one data set and the coefficients  $D$  and  $\beta$  are calculated for the complete data set. The coefficients obtained from the HS-equation are compared with those obtained using the Paris equation in Table 4 (Clerc et al. (2019a, b)). Generally, the  $\beta$  coefficient is much smaller than the  $m$  coefficient and the relative difference of the coefficient between the adhesive system is also less. Meaning, as explained by Jones et al. (2015) that if the data are used for design purposes, the error bound to the power coefficient by extrapolating remains relatively similar between samples or adhesive systems. The coefficients obtained for adhesively bonded wood are relatively similar to the one obtained by Jones et al. (2015) for composites in Mode II. Generally, slower crack growth is observed as the  $D$  coefficient is lower and the  $\beta$  coefficient higher for the several tested composites, but the  $A$  and  $G_{\text{thr}}$  remain relatively similar.

### 4 Discussion

#### 4.1 Sources of scatter

As shown in Fig. 9, the crack growth data and ERR data are associated with a relatively constant scatter over the complete duration of the fatigue test. For the

**Fig. 6** Data points of the three samples glued with the adhesive HB 110 are plotted in comparison with the mean fit obtained with the HS-analysis—the confidence range is given with 95% confidence interval

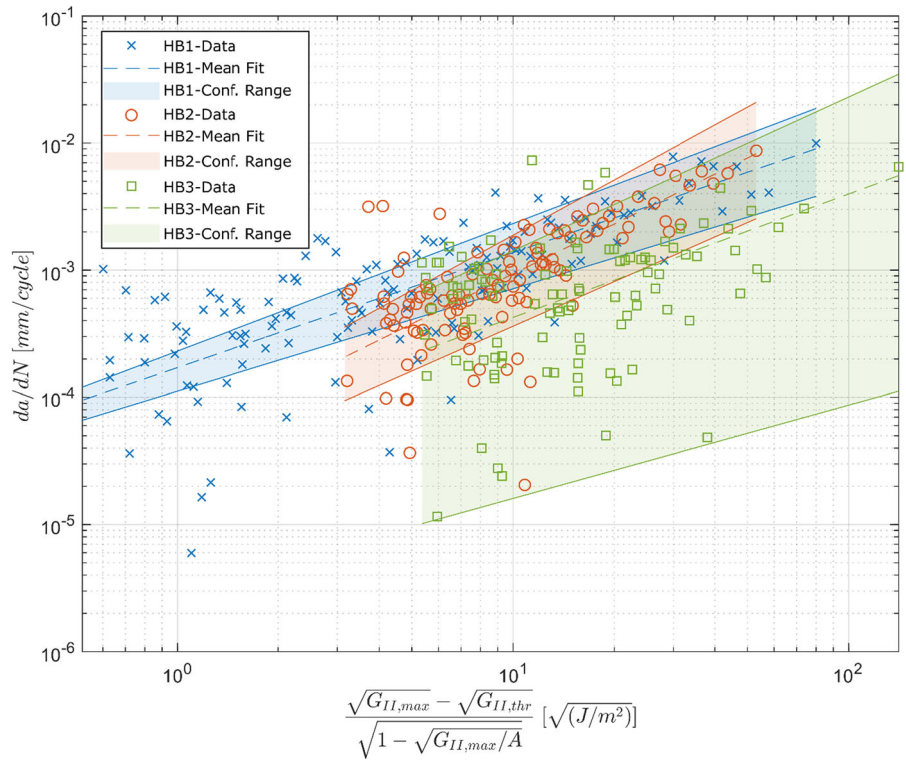


**Table 3** Hartman–Schijve coefficient for all tested samples

	Sample	A (J/m <sup>2</sup> )	G <sub>thr</sub> (J/m <sup>2</sup> )	D	β
HB 110	HB110-1a1	874 ± 9	315 ± 5	8.54E−06	1.73
	HB110-1a5	723 ± 9	246 ± 13	7.80E−06	1.95
	HB110-3a2	727 ± 18	306 ± 19	4.26E−05	1.71
PRF	PRF-3B3	885 ± 21	555 ± 10	5.81E−06	1.92
	PRF-3B4	876 ± 23	550 ± 6	4.94E−06	1.95
	PRF	880*	552*	N.A	N.A
VN 3158	VN1B4	1275 ± 8	287 ± 5	9.86E−04	0.64
	VNS2-2	1275 ± 14	145 ± 2	3.27E−04	1.26
	VNS2-3	1151 ± 5	134 ± 6	3.23E−04	1.45

Average value from PRF2 and PRF3 only

crack length a variation of approximately 5% of the average value is observed, for the ERR value a variation of below 2% of the average values is observed.

These observations confirm the estimation of the measurement accuracy presented in 2.6. Indeed, as the crack length is directly calculated from the compliance according to Eq. 4, the same accuracy can be expected. In comparison, the ERR values are calculated (according to Eq. 3) using only the maximum force per cycle. Therefore, the scatter of the results in

this case is lower. This also confirms that the main cause of measurement inaccuracy is due to the load and displacement measurement and the related measurement resolution. In addition to this relatively homogenous scatter, strong deviation of the crack length and ERR during a short amount of cycle can be observed. As these events are sporadic and associated to deviation higher than the measured extrinsic scatter, they can realistically be associated with intrinsic scatter due to the material heterogeneity.

**Fig. 7** Data points of the three samples glued with the adhesive VN 3158 are plotted in comparison with the mean fit obtained with the HS-analysis—the confidence range is given with 95% confidence interval

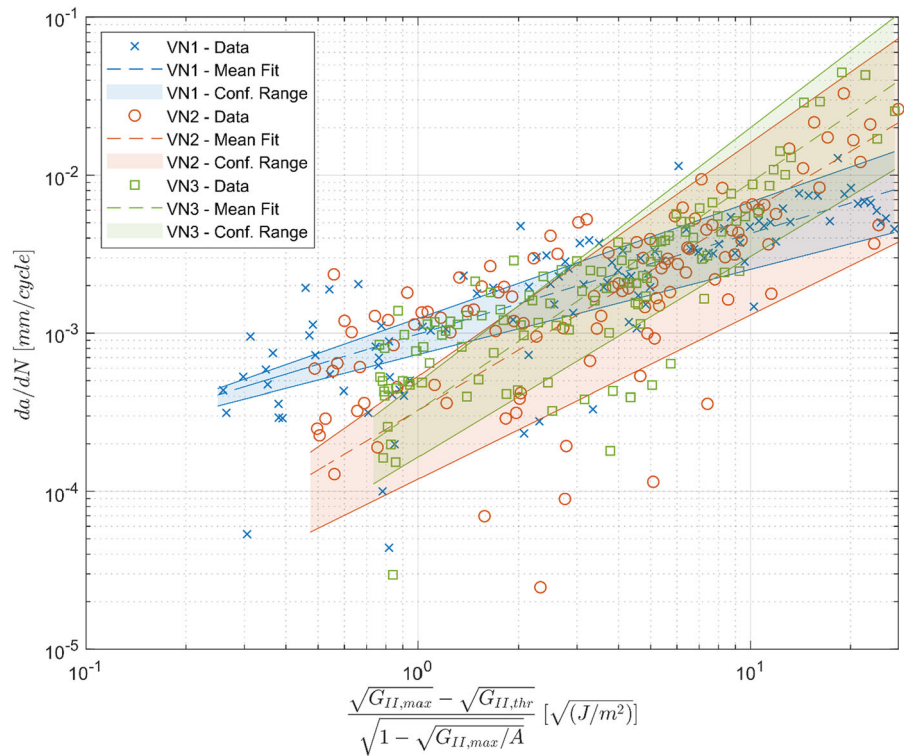


**Fig. 8** Data points of the three samples glued with the adhesive PRF are plotted in comparison with the mean fit obtained with the HS-analysis, the confidence range is given with 95% confidence interval

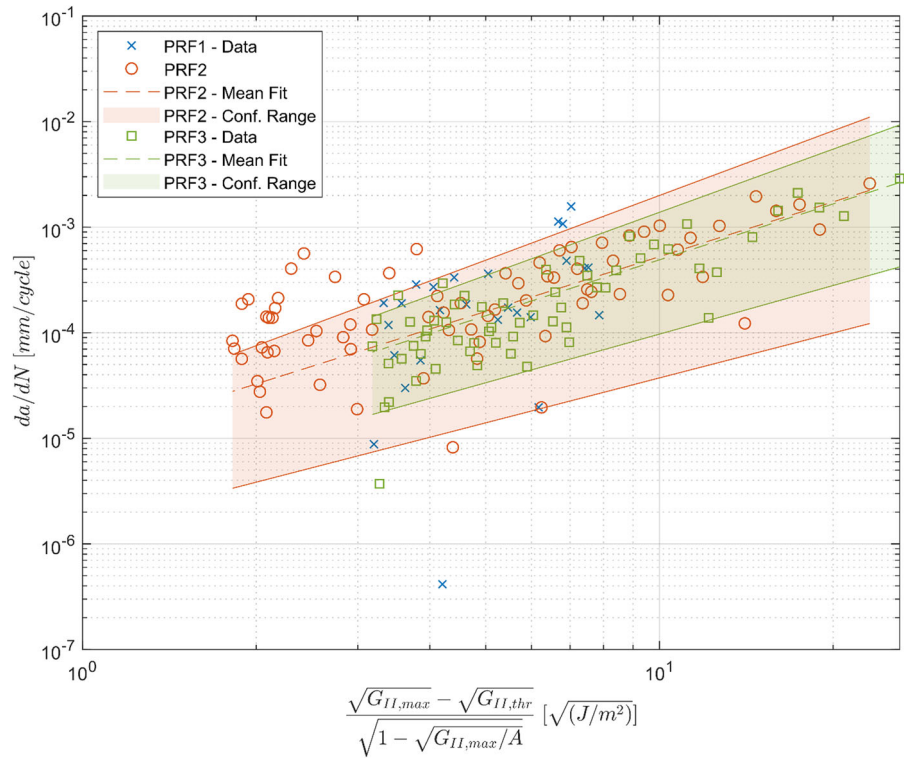


**Fig. 9** All data points from one adhesive system were plotted together with the corresponding fit using the HS-analysis—the confidence range is given with 95% confidence interval

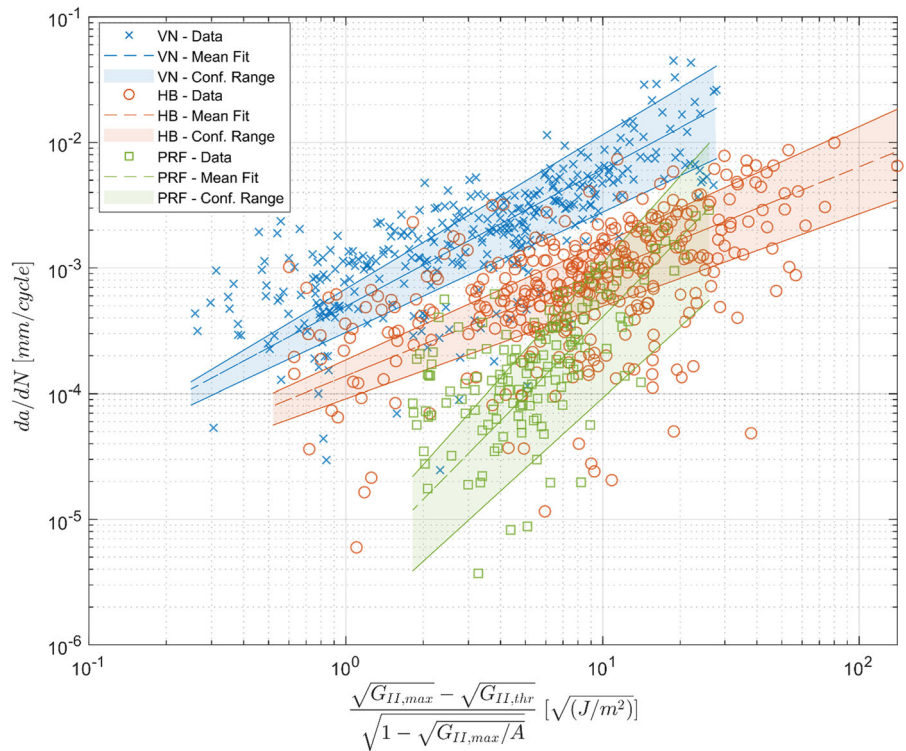


**Table 4** Comparison between Multi-sample fit (MS-fit) of the power-model coefficient between the Paris- and Hartmann–Schijve-equations

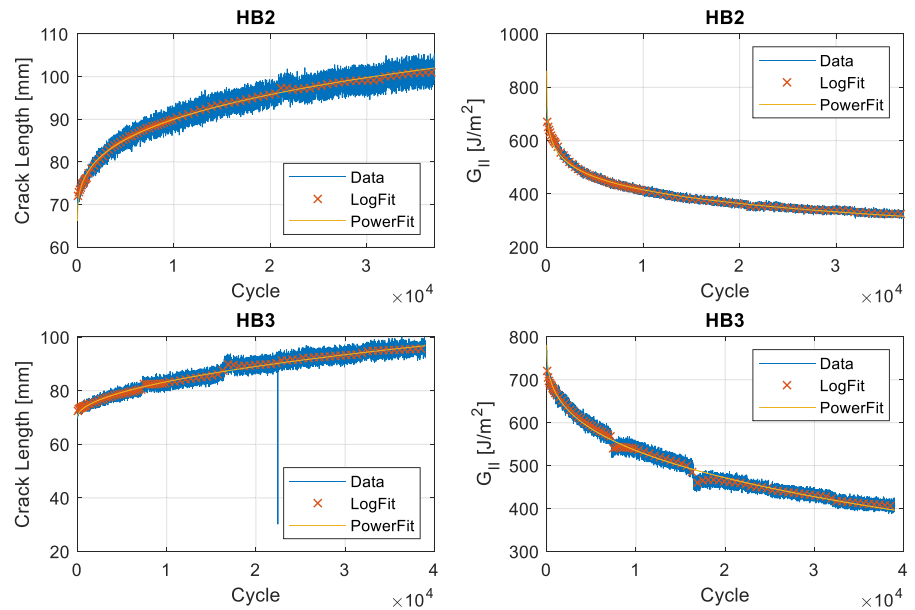
	Sample	C for Paris equ. D for HS equ.	m for Paris equ. $\beta$ for HS-equ.
Paris-equation	MS-fit-VN	5.76E-07	1.51
	MS-fit-HB	5.51E-13	3.44
	MS-fit-PRF	4.70E-42	13.33
Hartman–Schijve-equation	MS-fit-VN	4.94E-04	1.09
	MS-fit-HB	1.38E-04	0.83
	MS-fit-PRF	3.41E-6	2.08

For example, as can be seen in Fig. 6, the sample HB3 has a much higher scatter than the other HB samples. This higher scatter is probably due to two isolated non-homogenous crack growth events, one of them resulting in a significant spike in the data during the fatigue test. As visible in Fig. 10, at 8000 and 18,000 cycles approximately, a sudden crack growth and decrease of the ERR is observed for the sample HB3. Following the fast growth of the crack, the delamination length remains constant until the ERR needed for the further crack growth is reached. During this event, the crack growth increment per cycle becomes very small, and as the data are plotted chronologically;

this very slow crack growth is associated with scatter. In comparison, the sample HB2 shows a much more regular crack growth as visible in Fig. 10, hence the reduced scatter observed for these samples.

During the experiment, the machine had to be stopped for a short period, mainly to export results and hence free the memory of the acquisition system. It could be that these short interruptions may have influenced the compliance of the specimen through relaxation effects. For example, the machine was stopped at 22,000 cycles for the sample HB3 to export the preliminary results. In Fig. 10, at 22,000 cycles a small increase in the crack length and a very small decrease

**Fig. 10** Comparison of the crack growth and ERR values during the fatigue test of two different samples glued with adhesive HB 110 illustrating the non-regular behavior of the sample HB3 due to fast crack growth events (observed at 8000 and 18,000 cycles)



of the  $G_{II}$  value can be observed for the sample HB3. These modifications are however much smaller than the sporadic crack growth events at 7500 and 16,570 cycles presented before. The reasons for these sporadic events are not yet completely understood but could be due to non-uniform adhesive application and/or to heterogeneity in local morphology of the material. They are therefore associated with intrinsic scatter and should be considered in the safety factors determined from these tests in order to account for the specimen variability. It should, however, be recognized that the above mentioned factors influencing the scatter are obtained from laboratory test series and that these sources of scatter do not necessarily occur in service, where other sources may be present (Schijve 1994).

#### 4.2 Further considerations for reducing the scatter

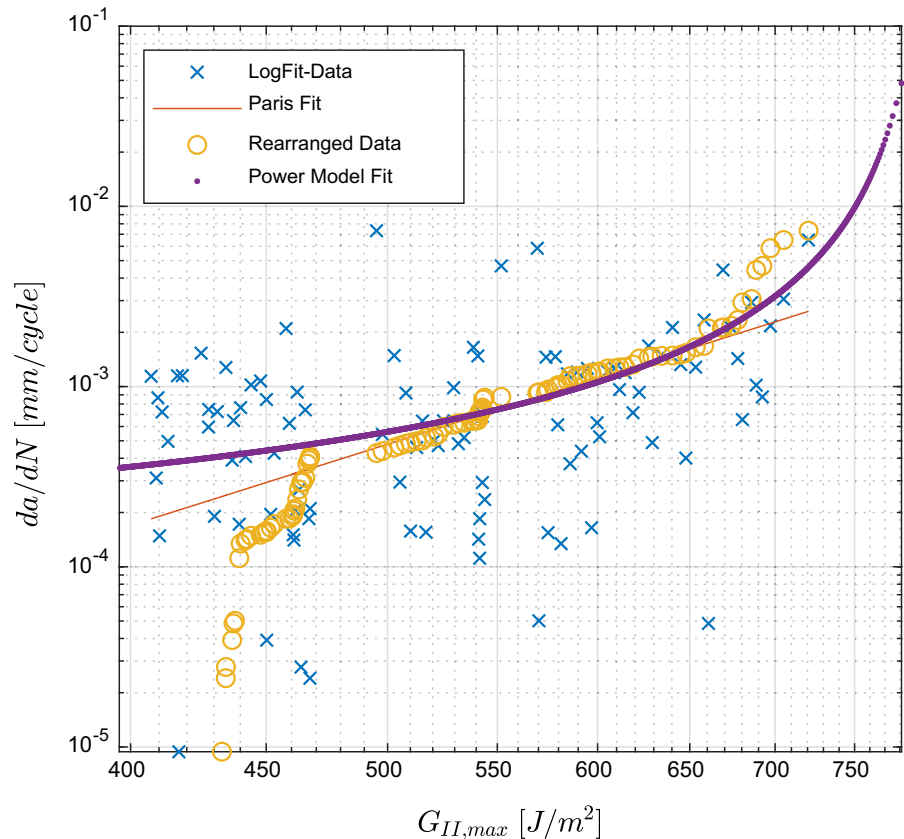
The problem of scatter is a frequent topic in fatigue testing. (Schijve 1994) mentioned that scatter encountered in S–N data is often a “nuisance” which can prevent the fitting of the data. An interesting solution to this was proposed by Gatto (1956) which consists in arranging the strength (S) values in descending order and the cycle (N) values in ascending order as ideally expected and to plot the obtained pairs as (S,N) values. Using this method, the scatter could be drastically reduced and the centroidal line could be localized immediately without

“mathematical treatment” of the data, which was probably appreciated at a time where computer usage was relatively scarce, but also to limit the risk of overfitting the data. This method also estimates the random variability of the population around its centroidal line by computing the difference between the experimental values and value of the rearranged coordinate. Hence, this is offering a new statistical variable for estimating the scatter of S–N curves. To the authors’ knowledge this method was never applied to fatigue crack growth data. Instead of the strength and cycle data, the crack growth rate and ERR could be plotted in ascending order as theoretically expected. This rearrangement method was compared to the power model fitting (fitting the crack growth and ERR with a power model of first order) in Fig. 11.

A very similar fit is observed between the rearranged data and the power model fit in the linear range of Fig. 11, between 470 and 700  $J/m^2$ . Outside this range, the deviations are important between both data reduction methods, as the power model is extrapolating the data along the same tendency whereas the rearranged data are showing an asymptotic decrease in the low ERR and increase for the high ERR, as ideally expected from a fatigue fracture test.

The Paris fit determined using the data reduction method presented by Clerc et al. (2019a,b) seems to match the rearranged data better than the power model fit. As the average difference between the rearranged

**Fig. 11** Comparison between the rearranged method and the Power Model fit on one data set plotted using the Paris Analysis illustrating the good correspondence of the three data reduction method between 470 and 700 J/m<sup>2</sup>



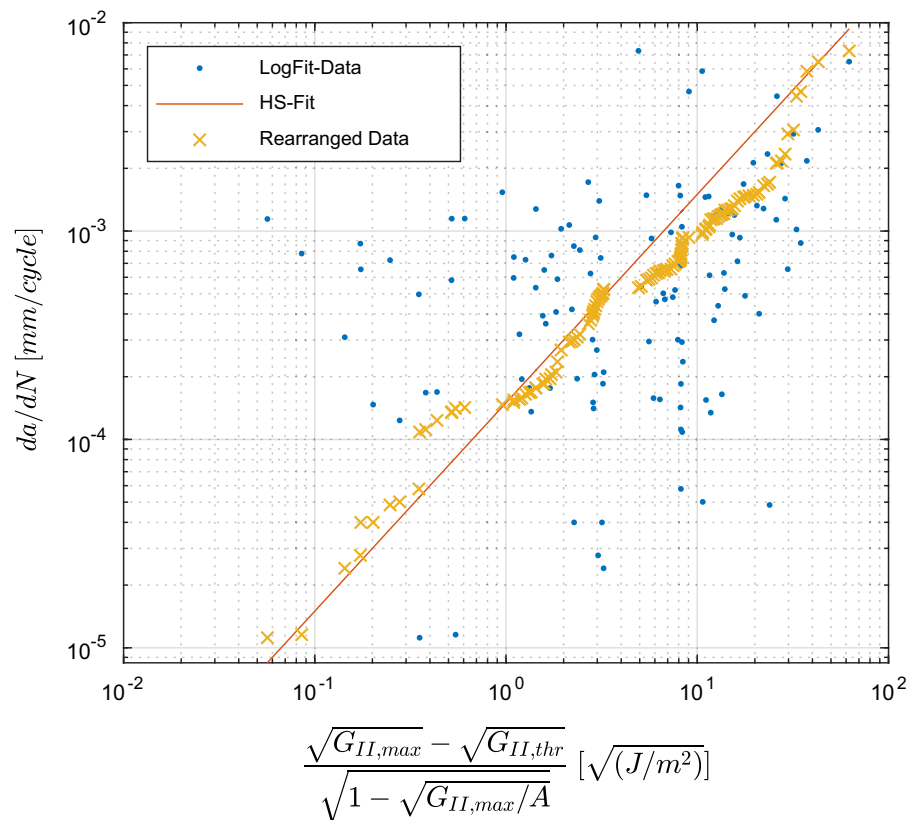
points and the original points is near zero for the crack growth and ERR values, it seems more appropriate to compute the absolute difference instead. This yields a value of 151 J/m<sup>2</sup> for the ERR values and 0.0013 mm/cycle for the crack growth rate. As mentioned by Gatto (1956), these values can be used as estimation of the scatter of the data.

The rearranged data plotted in Fig. 11 seem to follow the expected typical fatigue crack growth behavior. It is therefore interesting to investigate how the rearranged data are displayed using the HS-analysis.

It is possible to plot the rearranged data in a straight line that matches quite precisely the HS-fit line obtained from the LogFit Data by adjusting the  $G_{thr}$  and A values as shown in Fig. 12. However, it needs to be mentioned that the obtained A and  $G_{thr}$  values are different from those computed using the method described in Sect. 2.7. For example, Fig. 12 was plotted using a A-value of 730 J/m<sup>2</sup> and 430 J/m<sup>2</sup> for  $G_{thr}$ . In comparison, the A-value computed with the method described in 3.2 was  $727 \pm 18$  J/m<sup>2</sup> and  $306 \pm 19$  J/m<sup>2</sup> for  $G_{thr}$ . As the difference between both A-values is below the

standard deviation of 18 J/m<sup>2</sup> they can be considered similar. However, the difference between both  $G_{thr}$ -values is much higher than the standard deviation of 19 J/m<sup>2</sup>. To the question of which estimation of  $G_{thr}$  is the most accurate, several points need to be considered. The value of 430 J/m<sup>2</sup> is actually higher than the minimal recorded ERR during the test, in fact 15% of the data points displayed an ERR value lower than 430 J/m<sup>2</sup>. Also, after sorting the data in ascending order there is not necessarily a match corresponding to the real behavior of the specimen for each recorded value. Indeed, if a high crack growth is observed due to a hypothetical material heterogeneity or non-uniform adhesive application as discussed above, the theoretical high ERR corresponding to this crack growth rate does not necessarily exist in the data set. Instead, this crack growth rate will be plotted with an ERR value corresponding approximately to the same rank, leading therefore to a possible underestimation of the A value. After the fast crack growth, a slower delamination increase will be observed associated with low ERR until the general trend of the data is reached

**Fig. 12** Application of the rearranged data reduction method to the HS-analysis illustrating the potential of the this data reduction method to reduce the scatter and estimate the A and  $G_{II,thr}$  values



again. In this case, the slow crack growth rate will not necessarily be associated with the corresponding low ERR value leading this time to an overestimation of the ERR threshold value. Similar critics were formulated by Schijve (1994) considering the application of the method to S–N data. Nevertheless, it was shown that the rearrangement method proposed by Gatto (1956) can be successfully applied to fatigue crack growth data to reduce the scatter and obtain easily the centroidal line of the data. If this method is used to estimate the fatigue behavior outside the linear range, i.e. using the HS-analysis, the ERR threshold value will likely be overestimated, and the A value underestimated.

#### 4.3 Application of the HS-equation to a design guideline

One of the advantages of the HS-equation, is that the ERR threshold value is an explicit parameter of the equation and can be estimated. The ERR threshold value presented in this study was obtained for long crack and under constant amplitude loading. The influ-

ence of possible short crack effects, where a short crack (in comparison with a relevant microstructural scale of the material as defined in (ASTM E647)), grows at an unexpected high rate as discussed by Jones et al. (2014) for polymer composites should be investigated. To date and to the best knowledge of the authors, such effects have not been reported for wood materials or adhesively bonded wood joints. However, in analogy with fiber-reinforced polymer composites, this can a priori not be excluded and may effectively occur, even though its existence may be difficult to prove, among others, simply because of the large variability in wood morphology and properties. In order to estimate a valid value of the threshold below which no significant fatigue crack growth occurs, the conservative design approach discussed in detail by Jones et al. (2017) could be used. This approach, based on the (modified) Hartman–Schijve equation, consists of estimating an upper bound fatigue crack growth curve which encompasses all the experimental data. At the same time, a realistic experimental scatter can be determined. The ERR threshold value associated with this conservative fatigue crack

growth curve could then be reduced by two or three standard deviations depending on the required safety level. The value chosen for the safety factor would also have to accommodate the intrinsic scatter in the data due to limited measurement resolution (load and displacement from test machine) in the low load regime typically associated with near threshold delamination tests. Therefore, the consistency of the ERR threshold value should be verified as it can typically be expected that at low loads the extrinsic scatter will increase due to the uncertainty of the load and displacement measurements. However, even in this approach there is a further issue: for fiber-reinforced polymer composites, where specimens with unidirectionally aligned fibers are used in testing for design values, the safety factor may be overestimated due to effects of large-scale fiber bridging (as recently discussed by Yao et al. and Alderliesten et al.). In multidirectional fiber composites (mostly used in structural applications) the effective fiber-bridging may be significantly less than in the test coupons for determining the fracture behavior of the laminate and the design limits. The only exception noted in literature are wind rotor blades that consist of mainly unidirectional lay-up, where the large-scale fiber-bridging is effectively exploited in the design. In the adhesively bonded wood joints, fiber bridging does not occur as long as the delamination runs in the adhesive layer or at the adhesive-wood interface. If, however, the delamination fully or partially deviates into the wood layer adjacent to the adhesive bond-line, as observed for some types of adhesives (Clerc et al. 2019a, b), the same argument as for the wind rotor blade could be used, i.e., fiber bridging in the wood would contribute to slowing delamination propagation and this would be captured by the respective Hartman–Schijve data analysis (as shown by the Mode II fatigue fracture data presented in the manuscript). Therefore, the HS-type data analysis provides data ( $G_{\text{thr}}$  and ERR values with respective scatter) that can be used in the development of a future design guideline.

## 5 Conclusion

It was shown that the use of the HS-equation, despite the low number of samples analyzed in this feasibility study, yields plausible results for describing mode II fatigue fracture of wood adhesively bonded joints and that it represents a viable alternative to the Paris-

equation. Indeed, the advantages of the HS-equation are the following:

- Allows to estimate the ERR threshold and maximum values directly from fitting the data with the HS-equation
- The description is more physics-based as  $da/dN$  is proportional to a  $\sqrt{G}$ -term (i.e., directly proportional to  $K$ ) instead of to  $G$  and quasi-static critical ERR and threshold values are explicit parameters in the HS-equation
- For data plotted using the Paris-equation, it is difficult to estimate precisely whether the test data are all obtained from the linear crack growth part of the fatigue fracture test. This does not matter for data plotted using the HS-equation as the complete data-set is linearized by the equation.
- The lower power-law coefficient in the HS-equation (compared to the Paris-equation) and, in addition, having a similar exponent coefficient between different adhesive systems means that the same design methodology can be used, as the errors will remain in the same range.

Despite these advantages, the fitting process needed to determine the four parameters of the HS-equation is relatively cumbersome and somewhat subjective for data showing a large scatter. To simplify the fitting process, an automatic method which can be used even if significant scatter of the data is seen was successfully applied to wood specimens bonded with three different adhesives types. Additionally, an analysis a posteriori of the scatter origin has shown that it can differentiate between extrinsic and intrinsic scatter. The main cause of extrinsic scatter is attributed to limited measurement resolution at low levels of load and displacement. The intrinsic scatter for adhesively bonded wood is likely due to sporadic events where a sudden faster crack growth was observed, probably caused by a non-uniform adhesive application or heterogeneity in local morphology of the adherends.

The main advantages of the HS-equation appear for an application in design guidelines. However, before the  $A$  and  $G_{\text{thr}}$  values presented here can be used in design applications, several issues should first be investigated. One such question is, how the number of cycles and the corresponding ERR value influence the calculated  $G_{\text{thr}}$  value. Also, further tests would be necessary to explore the link between the  $A$ -value and the ERR measured during quasi-static test, the influence of pos-

sible short crack effects on the measured threshold ERR and the variation and intrinsic scatter of the  $G_{thr}$ -value.

**Acknowledgements** The authors thank the Swiss Innovation Agency for the financial support (Project 18958.1), as well as Henkel AG for providing IC-PUR adhesive. Furthermore, the assistance of Mr. Daniel Völki for the test machine setup and data acquisition is gratefully acknowledged.

**Author contributions** All authors contributed to the study conception and design. Material preparation, data collection and analysis were performed by GC. The first draft of the manuscript was written by GC and AJB and all authors commented on previous versions of the manuscript. All authors read and approved the final manuscript.

#### Compliance with ethical standards

**Conflict of interest** The authors declare that they have no conflict of interest.

#### References

- Aicher S, Christian Z (2015) Fatigue behavior of wood and glued wood components. 21. Internationales Holzbau-Forum IHF Alderliesten RC, Brunner AJ, Pascoe JA (2018) Cyclic fatigue fracture of composites: what has testing revealed about the physics of the processes so far? *Eng Fract Mech* 203:186–196. <https://doi.org/10.1016/j.engfracmech.2018.06.023>
- Bachtiar EV, Clerc G, Brunner AJ, Kaliske M, Niemz P (2017) Static and dynamic tensile shear test of glued lap wooden joint with four different types of adhesives. *Holzforschung* 71:2751. <https://doi.org/10.1515/hf-2016-0154>
- Clerc G, Brunner AJ, Jossset S, Niemz P, Pichelin F, van de Kuilen JWG (2019a) Adhesive wood joints under quasi-static and cyclic fatigue fracture Mode II loads. *Int J Fatigue* 123:40–52. <https://doi.org/10.1016/j.ijfatigue.2019.02.008>
- Clerc G, Sause MGR, Brunner AJ, Niemz P, van de Kuilen JWG (2019b) Fractography combined with unsupervised pattern recognition of acoustic emission signals for a better understanding of crack propagation in adhesively bonded wood. *Wood Sci Technol*. <https://doi.org/10.1007/s00226-019-01136-6>
- Gatto F (1956) New statistical methods applied to the analysis of fatigue data. In: Weibull W, Odqvist FKG (eds) IUTAM Colloquium on Fatigue, pp 66–77
- Hartman A, Schijve J (1970) The effects of environment and load frequency on the crack propagation law for macro fatigue crack growth in aluminium alloys. *Eng Fract Mech* 1:615–631. [https://doi.org/10.1016/0013-7944\(70\)90003-2](https://doi.org/10.1016/0013-7944(70)90003-2)
- Jones R, Pitt S, Bunner AJ, Hui D (2012) Application of the Hartman–Schijve equation to represent Mode I and Mode II fatigue delamination growth in composites. *Compos Struct* 94:1343–1351. <https://doi.org/10.1016/j.compstruct.2011.11.030>
- Jones R, Stelzer S, Brunner AJ (2014) Mode I, II and mixed Mode I/II delamination growth in composites. *Compos Struct* 110:317–324. <https://doi.org/10.1016/j.compstruct.2013.12.009>
- Jones R, Hu W, Kinloch AJ (2015) A convenient way to represent fatigue crack growth in structural adhesives. *Fatigue Fract Eng Mater Struct* 38:379–391. <https://doi.org/10.1111/ffe.12241>
- Jones R, Kinloch AJ, Michopoulos JG, Brunner AJ, Phan N (2017) Delamination growth in polymer-matrix fibre composites and the use of fracture mechanics data for material characterisation and life prediction. *Compos Struct* 180:316–333. <https://doi.org/10.1016/j.compstruct.2017.07.097>
- Kyanka GH (1980) Fatigue properties of wood and wood composites. *Int J Fract* 16:609–616
- Lewis WC (1960) Design consideration of fatigue in timber structures. *Am Soc Civ Eng* 86:15–23
- Paris P, Erdogan F (1963) A critical analysis of crack propagation laws. *J Basic Eng* 85:528–533. <https://doi.org/10.1115/1.3656900>
- Schijve J (1994) Fatigue predictions and scatter. *Fatigue Fract Eng Mater Struct* 17:381–396
- Simon I, Banks-Sills L, Fourman V (2017) Mode I delamination propagation and R-ratio effects in woven composite DCB specimens for a multi-directional layup. *Int J Fatigue* 96:237–251. <https://doi.org/10.1016/j.ijfatigue.2016.12.005>
- Smith I, Landis E, Gong M (2003) *Fracture and fatigue in wood*. Wiley, Winchester
- Stelzer S, Brunner AJ, Argüelles A, Murphy N, Cano GM, Pinter G (2014) Mode I delamination fatigue crack growth in unidirectional fiber reinforced composites: results from ESIS TC4 round-robins. *Eng Fract Mech* 116:92–107. <https://doi.org/10.1016/j.engfracmech.2013.12.002>
- Yao L, Alderliesten RC, Jones R, Kinloch AJ (2018) Delamination fatigue growth in polymer-matrix fibre composites: a methodology for determining the design and lifing allowables. *Compos Struct* 196:8–20. <https://doi.org/10.1016/j.compstruct.2018.04.069>

**Publisher's Note** Springer Nature remains neutral with regard to jurisdictional claims in published maps and institutional affiliations.